JACS
JOURNAL OF THE AMERICAN CHEMICAL SOCIETY

COMMUNICATION

pubs.acs.org/JACS

Multifunctional Graphene/Platinum/Nafion Hybrids via Ice Templating

Luis Estevez,[†] Antonios Kelarakis,[†] Qianming Gong,[†,‡] Eman Husni Da'as,[†,§] and Emmanuel P. Giannelis*[,†]

[†]Department of Materials Science and Engineering, Cornell University, Ithaca, New York 14853, United States

[‡]Department of Mechanical Engineering, Tsinghua University, Beijing 100084, China

[§]Department of Materials Science and Engineering, King Abdullah University of Science and Technology, Thuwal 23955-6900, Kingdom of Saudi Arabia

Supporting Information

ABSTRACT: We report the synthesis of multifunctional hybrids in both films and bulk form, combining electrical and ionic conductivity with porosity and catalytic activity. The hybrids are synthesized by a two-step process: (a) ice templation of an aqueous suspension comprised of Nafion, graphite oxide, and chloroplatinic acid to form a microcellular porous network and (b) mild reduction in hydrazine or monosodium citrate which leads to graphene-supported Pt nanoparticles on a Nafion scaffold.

Macroporous materials have numerous applications that include molecular filtration, biological scaffolds, microfluidics, photovoltaics, organic electronics, and fuel cells.[1−5] Among various methods developed for the preparation of macroporous materials, freeze-casting has attracted considerable attention, since it is an inexpensive and versatile technique that exploits the controlled crystallization of a suspension to induce ordering.[6−10] As the solvent freezes, spontaneous phase segregation confines the dispersed particles to the area between the crystals. Once the structure is set, the frozen template is sublimed, leaving behind a three-dimensional network of macropores similar to cellular foams. Work to date has emphasized freeze-casting colloidal suspensions of ceramic nanoparticles, occasionally in the presence of an organic binder.[7−11] Other work has focused on skeletons based on poly(vinyl alcohol) (PVA), poly(lactic acid), poly(vinyl laurate), poly(acrylamide), or polystyrene, in the absence or in the the presence of inorganic nanofillers (silica, clay, ceria, carbon nanotubes).[12−20]

Here we demonstrate a novel strategy to prepare electrically conductive, macroporous hybrids in both films and bulk form comprised of graphene-supported platinum nanoparticles well-dispersed within an ionomer. While the technique is applicable to a variety of systems, we focus here on an aqueous suspension of Nafion, well-dispersed graphite oxide (GO) nanosheets, and chloroplatinic acid. After cryo-processing and structure formation, the samples were treated with hydrazine or monosodium citrate to allow the *in situ* reduction of GO and chloroplatinic acid to graphene nanosheets (GS) and Pt nanoparticles, respectively, as shown in Scheme 1.

There are two main differences in our approach to prepare freeze-cast hybrids from those reported previously. First, we demonstrate the synthesis of multifunctional systems that combine electrical and ionic conductivity with porosity and catalytic activity. Second, our approach exploits the use of an aqueous dispersion containing two types of nanoparticle precursors, rather than the nanoparticles themselves. This approach not only can effectively circumvent problems arising from limited dispersibility of the desired nanoparticles in a given solvent/polymer system but also allows the successive or simultaneous evolution of a number of different types of nanoparticles by virtue of the large free space of the sponge-like network.

In a previous report, ice-templated Nafion was used as the support medium for the deposition of PtRu nanoparticles, but the morphology of the scaffolds was not studied.[17] Nafion is widely used as an ionomer membrane in energy converters and has also been explored for the development of biosensors and electrocatalysts due to its biocompatible, yet antifouling, character coupled with its excellent electrochemical performance.[18−20] Nafion is comprised of a rigid, highly hydrophobic Teflon-like backbone with hydrophilic perfluoroether side chains bearing terminal sulfonic acid groups.[21] This molecular design imparts excellent morphological stability and long-term durability, while the interconnectivity between the ionic groups to form clusters facilitates the transport of ions and polar molecules.

The development of structured systems composed of Nafion, GS, and platinum is of significant technological importance for applications ranging from sensors[22] to membrane electrode assemblies in fuel cells.[23] With respect to fuel cells, the macroporous structure presented in this work can give rise to extensive triple phase boundaries, which are the contact points in a membrane electrode assembly between the gas reactants (flowing through the pores), the ionic conductor (Nafion), and the catalyst (Pt) adsorbed to an electronically conductive support (graphene).[23]

Nafion suspensions in water thicken considerably when subjected to prolonged and vigorous mechanical stirring that is required in order to ensure a homogeneous dispersion (especially in the presence of nanofillers, *vide infra*). Although investigation of this rheopectic behavior[24,25] falls beyond the scope of the present study, we note that it has a significant impact on the morphology of the resultant cryostructured scaffolds. In particular, the scaffolds derived from the unsheared Nafion dispersions are composed of well-defined ribbons periodically interconnected with

Received: January 16, 2011
Published: April 04, 2011

dx.doi.org/10.1021/ja200244s | *J. Am. Chem. Soc.* 2011, 133, 6122–6125

Scheme 1. Schematic Showing Ice Templation To Synthesize a Nafion Scaffold with Pt and Graphene Nanosheet Precursors Revealed upon Reduction

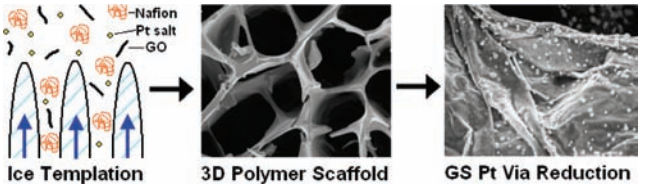

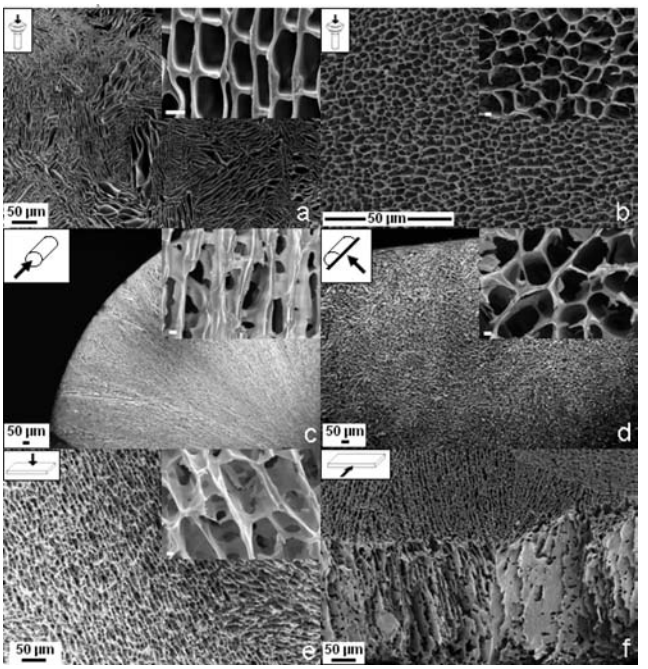

Figure 1. SEM images of cryostructured Nafion scaffolds. Spherical samples derived from unsheared (a) and sheared aqueous suspensions (b). Cylindrical samples viewed along the axis (c) or across the thickness (d). Deposited films viewed across the thickness (e) or the edge plane (f). Insets at the top right of each image show a high-resolution SEM image, with each scale bar representing 1 μm.

transverse pillars (Figure 1a). In contrast, the scaffolds prepared from the sheared, more viscous Nafion dispersion show instead an interconnected porous 3D geometry (Figure 1b). Evidently, the more viscous sheared sample seems to favor the formation of larger ice crystals that promote branching. In addition to viscosity, the structure/morphology of the sample is determined by the speed of the ice front, the particle size of the species in dispersion, the osmotic pressure, and the surface tension of the suspension.[8,9]

The discussion below focuses on scaffolds derived from sheared aqueous Nafion suspensions (10−15 wt %). At these concentrations, fairly robust, crack-free scaffolds with various geometries that show minimal dissolution in water are obtained (see Supporting Information (SI), Figure S1). The Nafion suspensions were plunged into the nitrogen slurry rather than gradually immersed in it, as is typically the case in unidirectional ice templating.[12] The morphologies obtained are highly anisotropic (Figure 1) due to the intrinsic temperature gradient. For cylindrical samples, the ice front travels along the radius of the cylinder, from the periphery of the cylinder toward the center (Figure 1c,d). Similar morphologies arising from the ice templating are also present in the film samples, which show lamella arrays perpendicular to the film surface (Figure 1e,f).

Along with the macroporosity induced by cryocasting seen in Figure 1, Nafion also possesses inherent nanoscale porosity arising from the clustering of its ionic domains.[21] Both nano- and macroporosity can be traced back to the presence of water. Nafion's nanopores tend to absorb large amounts of water, resulting in reversible swelling, but their size and connectivity seem to be independent of processing. In contrast, the macropores are formed as part of the ice templation, and their size and morphology directly depend on the speed of ice crystallization and the particle size of the species in the dispersion.

In addition to single-component cellular solids, hybrid samples containing well-dispersed GS and platinum nanoparticles were prepared following a similar approach. A substrate was immersed in a homogeneous aqueous dispersion consisting of Nafion, GO, and chloroplatinic acid (alternatively, for bulk samples the dispersion was carefully loaded into the mold) and was subject to freeze-casting. The resulting macroporous film was treated with a reducing agent (hydrazine or monosodium citrate) to allow chemical reduction of GO and chloroplatinic acid to GS and Pt nanoparticles, respectively. We have recently demonstrated that even in solid Nafion samples, the nanoporosity due to the presence of ionic domains allows sufficient access of the reducing agent into the sample despite the lack of macroporosity.[26] In this work the macroporous nature of the samples further facilitates the diffusion of the reducing agent throughout the polymeric skeleton, so that the nanoparticle precursors, even those that reside in the vicinity of the substrate, can be readily accessed (*vide infra*). Thus far, the use of precursors to ice-templated structures has been limited to using polycarbosilane to prepare SiC ceramic scaffolds with desired morphology[27,28] and polycondensation of tetramethoxysilane within PVA cryogels.[29] Additionally, *in situ* polymerization of *N*-isopropylacrylamide within cryostructured clay foams has been described.[30] In a distinctly different approach, magnetic nanoparticles along the surface of the nanofibrils were deposited when a cellulose aerogel was immersed in an aqueous solution of $FeSO_4/CoCl_2$ and heat-treated at 90 °C.[31] To our knowledge, this is the first time that a one-step redox reaction has been used to transform two precursors to the corresponding nanoparticles.

A Nafion/GS/Pt film thus prepared was carefully sectioned at three different thicknesses to allow scanning electron microscopy (SEM) imaging of its outer surface, the middle, and near the substrate. The SEM images suggest a homogeneous distribution of the inorganic nanosheets and the platinum nanoparticles within the macroporous scaffold, even in the section closest to the substrate. Individual graphene nanosheets on the surface of the Nafion can be clearly identified by virtue of their characteristic crumpled texture (Figure 2a). After hydrazine treatment, it can be seen that the majority of platinum nanoparticles, with a size of 50−100 nm, are attached to the surface of graphene sheets (Figure 2b). This observation points to the ability of the (initially present) oxygen atoms to act as anchoring points for the absorption of chloroplatinic acid[32] and/or the efficacy of the defect sites of GS to nucleate Pt nanoparticles.[33] Alternatively, when monosodium citrate is used instead of hydrazine as the reducing agent (and otherwise following an identical protocol), much smaller platinum nanoparticles, with an average diameter close to 10 nm, are obtained (Figure 2d,e).

dx.doi.org/10.1021/ja200244s |*J. Am. Chem. Soc.* 2011, 133, 6122–6125

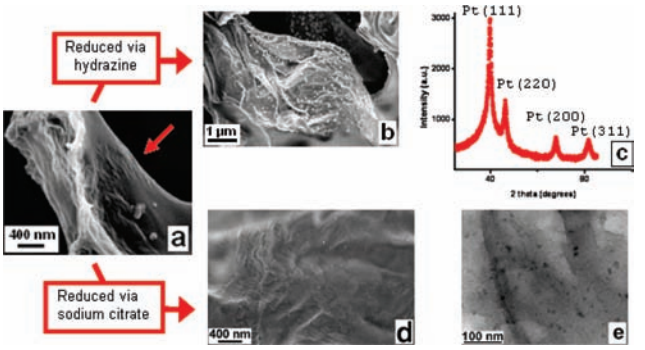

Figure 2. (a) SEM image of a freeze-cast Nafion/GS/Pt film showing the presence of graphite oxide nanosheets (arrow) on the surface of the macropores. (b) Platinum nanoparticles deposited on the surface of graphene, after hydrazine treatment, and (c) their XRD spectra. (d,e) SEM and TEM images respectively of platinum nanoparticles deposited on the surface of graphene, after treatment with monosodium citrate.

The X-ray diffraction pattern in Figure 2c exhibits diffraction peaks at $2\theta = 39.7°$, 46.3°, 67.4°, and 81.3° that can be identified as the Pt (111), Pt (200), Pt (220), and Pt (311) reflections of the platinum face-centered cubic crystals.[34] The elemental spectra obtained by energy-dispersive X-ray spectroscopy, shown in SI Figure S5, confirm the coexistence of Cl and Pt before reduction and the complete removal of Cl after chemical treatment. Taken together, the experimental evidence supports the presence of platinum nanoparticles after chemical reduction of the chloroplatinic acid. Previous reports suggested that GS can function as an excellent supporting platform for Pt nanoparticles, inhibiting their agglomeration and stabilizing their catalytic performance[22,35−38] due to its much higher surface-to-mass ratio compared to all others carbon supports (e.g., carbon black, carbon nanotubes, and carbon nanofibers). Cyclic voltametry (SI Figure S8) confirms that the platinum nanoparticles are catalytically active for the electrooxidation of methanol. Their catalytic activity is consistent with their average size of 50−100 nm.

Under anhydrous conditions, the ionic conductivity of Nafion is fairly low, and thus, a meaningful comparison between the electronic conductivities of the various samples can be made, provided that they have similar geometry and porosity. For convenience, we have tested the resistivity of cylindrical samples composed of Nafion/GO prior to and after hydrazine treatment at low relative humidity (<1 ppm). The resistance of the non-reduced Nafion/GO exceeds the upper detection limit of our device (~200 MΩ). After hydrazine treatment the resistance falls in the range of 10−20 kΩ. Thus, hydrazine treatment results in at least 4 orders of magnitude decrease in resistance, consistent with extensive chemical reduction of the insulating GO to more conducting graphene. Taking into account the high pore volume of the sample (~92 wt %) and applying the additivity rule, we estimate the electronic conductivity of the solid hybrid to be on the order of 1 S/m, in good agreement with values reported previously for Nafion/GS nanocomposites.[26] We note that the high electronic conductivity of the cellular Nafion/GS hybrid effectively prevents the accumulation of electronic charges at its surface during SEM imaging, as opposed to the (nonreduced) Nafion/GO sample that requires sputtering with an electronically conductive material to minimize charging effects during imaging (see SI Figure S5). Electronic conductivity induced by carbon nanotubes[6,40,41] or carbon black[13] has been reported in various cryostructured scaffolds.

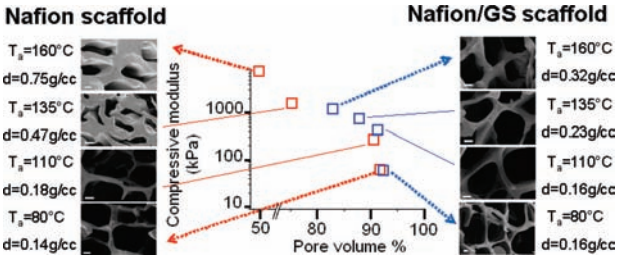

Figure 3. Compressive modulus as a function of the pore volume of cylindrical neat Nafion and Nafion/GS scaffolds that have been subject to thermal annealing (for 1 h) at the indicated temperatures (T_a). The data points are correlated with the SEM pictures of the corresponding annealed scaffolds, where the scale bar represents 1 μm. The densities of the scaffolds are also indicated.

The mechanical properties of the materials were evaluated using compression testing. SI Figure S6 shows typical compressive stress−strain plots for our samples. In general, the stress−strain curves exhibit a behavior typical of cellular solids. At small strains the material behaves elastically and the slope of the curve equals the compressive modulus of the material. At higher strains the material compacts gradually until it starts collapsing and the stress starts to increase sharply. The morphology and, thus, the mechanical response of the samples can be fine-tuned by thermal annealing. The modulus of the sample annealed at 80 °C (e.g., following our standard preparation protocol) is 60 kPa, despite its high pore volume (>90%). The sample shows no structural changes after annealing at $T_a = 95$ °C for a period of several days (see SI Figure S7). However, upon annealing at temperatures close to or above the glass transition of Nafion ($T_g \approx 120$ °C[39]) for 1 h, the density and cell thickness increase monotonically with annealing temperature, resulting in significant mechanical reinforcement (Figure 3). The compressive modulus and the pore volume of the sample annealed at 160 °C are 7.6 MPa and 49.2 vol %, respectively. The corresponding compressive moduli of the Nafion/GS hybrids are somewhat higher than those for neat Nafion, suggesting that incorporation of GS provides some degree of reinforcement. Interestingly, the thermally induced structural rearrangements observed in neat Nafion (vide supra) are greatly suppressed in the Nafion/GS hybrids (Figure 3). This behavior can be attributed to the large increase in T_g of Nafion in the presence of inorganic nanoplatelets (by as much as 50 °C)[24] and the formation of a percolated network of nanofillers that enhances the thermomechanical stability of the scaffold.

In summary, we report a novel approach to prepare electrically conductive, macroporous hybrids in both films and bulk form comprised of graphene-supported platinum nanoparticles well-dispersed within an ionomer. The films can be deposited directly onto the surface of any substrate, simply by dip-coating followed by freeze-casting. The method is simple, scalable, and applicable to a variety of systems. The microcellular scaffolds combine high levels of ionic (Nafion) and electronic (GS) conductivity along with catalytic activity (Pt) and, thus, are ideal candidates for fuel cell applications and biosensors.

■ ASSOCIATED CONTENT

Supporting Information. Detailed experimental procedures, macroscopic pictures of samples, EDS spectra before and after hydrazine treatment, complete stress−strain curves, and

characterization methods. This material is available free of charge via the Internet at http://pubs.acs.org.

AUTHOR INFORMATION

Corresponding Author
epg2@cornell.edu

ACKNOWLEDGMENT

The authors thank Scott Gilje of Northrop Grumman Space Technology for providing the graphite oxide used, Dr. Deli Wang for electrochemistry expertise, and John Grazul of the Cornell Center for Materials Research for helpful discussions regarding the cryogenic techniques. We acknowledge support from the Energy Materials Center at Cornell, an Energy Frontier Research Center funded by the U.S. Department of Energy, Office of Science, Office of Basic Energy Sciences, under Award No. DE-SC0001086. This publication is based on work supported in part by Award No. KUS-C1-018-02 from King Abdullah University of Science and Technology.

REFERENCES

(1) Davis, M. E. *Nature* **2002**, *417*, 813.
(2) Butler, R.; Hopkinson, I.; Cooper, A. I. *J. Am. Chem. Soc.* **2003**, *125*, 14473.
(3) Zhang, H.; Long, J.; Cooper, A. I. *J. Am. Chem. Soc.* **2005**, *127* 13482.
(4) Arachchige, I. U.; Brock, S. L. *J. Am. Chem. Soc.* **2007**, *129*, 1840.
(5) Rolison, D. R. *Science* **2003**, *299*, 1698.
(6) Gutiérrez, M. C.; Ferrer, M. L.; del Monte, F. *Chem. Mater.* **2008**, *20*, 634.
(7) Deville, S.; Saiz, E.; Nalla, R. K.; Tomsia, A. P. *Science* **2006**, *311*, 515.
(8) Deville, S.; Maire, E.; Bernard-Granger, G.; Lasalle, A.; Bogner, A.; Gauthier, C.; Leloup, J.; Guizard, C. *Nat. Mater.* **2009**, *8*, 966.
(9) Deville, S. *Adv. Eng. Mater.* **2008**, *10*, 155.
(10) Munch, E.; Saiz, E.; Tomsia, A. P.; Deville, S. *J. Am. Ceram. Soc.* **2009**, *92*, 1534.
(11) Halloran, J. *Science* **2006**, *311*, 479.
(12) Zhang, H.; Hussain, I.; Brust, M.; Butler, M. F.; Rannard, S. P.; Cooper, A. I. *Nat. Mater.* **2005**, *4*, 787.
(13) Colard, C. A. L.; Cave, R. A.; Grossiord, N.; Covington, J. A.; Bon, S. A. F. *Adv. Mater.* **2009**, *21*, 2894.
(14) Gutierrez, M. C.; Garcia-Carvajal, Z. Y.; Jobbagy, M.; Rubio, F.; Yuste, L.; Rojo, F.; Ferrer, M. L; de Monte, F. *Adv. Funct. Mater.* **2007**, *17*, 3505.
(15) Gawryla, M. D.; Liu, L.; Grunlan, J. C.; Schiraldi, D. A. *Macromol. Rapid Commun.* **2009**, *30*, 1669.
(16) Alhassan, S. M.; Qutubuddin, S.; Schiraldi, D. *Langmuir* **2010**, *26*, 12198.
(17) Arbizzani, C.; Beninati, S.; Manferrari, E.; Soavi, F.; Mastragostino *J. Power Sources* **2006**, *161*, 826.
(18) Turner, R. F. B.; Harrison, D. J.; Rajotte, R. V. *Biomaterials* **1991**, *12*, 361.
(19) Madaras, M. B.; Buck, R. P. *Anal. Chem.* **1996**, *68*, 3832.
(20) Galeska, I.; Chattopadhyay, D.; Moussy, F.; Papadimitrakopoulos, F. *Biomacromolecules* **2000**, *1*, 202.
(21) Mauritz, K. A.; Moore, R. B. *Chem. Rev.* **2004**, *104*, 4535.
(22) Lu, J.; Do, I.; Drzal, L. T.; Worden, R. M.; Lee, I. *ACS Nano* **2008**, *9*, 1825.
(23) Litster, S.; McLean, G. *J. Power Sources* **2004**, *130*, 61.
(24) Matsuo, T.; Pavan, A.; Peterlin, A.; Turner, D. T. *J. Colloid Interface Sci.* **1967**, *24*, 241.
(25) Narh, K. A.; Barham, P. J.; Keller, A. *Macromolecules* **1982**, *15*, 464.
(26) Ansari, S.; Kelarakis, A.; Estevez, L.; Giannelis, E. P. *Small* **2010**, *6*, 205.
(27) Yoon, B. H.; Lee, E. J.; Kim, H. E.; Koh, Y. H. *J. Am. Ceram. Soc.* **2007**, *90*, 1753.
(28) Yoon, B. H.; Park, C. S.; Kim, H. E.; Koh, Y. H. *J. Am. Ceram. Soc.* **2007**, *90*, 3759.
(29) Lozinsky, V. I.; Bakeeva, I. V.; Presnyak, E. P.; Damshkaln, L. G.; Zubov, V. P. *J. Appl. Polym. Sci.* **2007**, *105*, 2689.
(30) Bandi, S.; Bell, M.; Schiraldi, D. A. *Macromolecules* **2005**, *38*, 9216.
(31) Olsson, R. T.; Azizi Samir, M. A. S.; Salazar-Alvarez, G.; Belova, L.; Strom, V.; Berglund, L. A.; Ikkala, O.; Nogues, J.; Gedde, U. W. *Nature Nanotechnol.* **2010**, *5*, 584.
(32) Antolini, E. *J. Mater. Sci.* **2003**, *38*, 2995.
(33) Aktary, M.; Lee, C. E.; Xing, Y.; Bergens, S. H.; McDermott, M. T. *Langmuir* **2000**, *16*, 5837.
(34) Li, W.; Waje, M.; Chen, Z.; Larsen, P.; Yan, Y. *Carbon* **2010**, *48*, 995.
(35) Seger, B.; Kamat, P. V. *J. Phys. Chem. C* **2009**, *113*, 7990.
(36) Shang, N.; Papakonstantinou, P.; Wang, P.; Silva, S. R. P. *J. Phys. Chem. C* **2010**, *114*, 15837.
(37) Guo, S.; Wen, D.; Zhai, Y.; Dong, S.; Wang, E. *ACS Nano* **2010**, *4*, 3959.
(38) Dong, L. F.; Gari, R. R. S.; Li, Z.; Craig, M. M.; Hou, S. F. *Carbon* **2010**, *48*, 781.
(39) Alonso, R. H.; Estevez, L.; Lian, H. Q.; Kelarakis, A.; Giannelis, E. P. *Polymer* **2009**, *50*, 2402.
(40) Zou, J.; Liu, J.; Karakoti, A. S.; Kumar, A; Joung, D.; Li, Q.; Khondaker, S. I.; Seal, S.; Zhai, L. *ACS Nano* **2010**, *12*, 7293.
(41) Kwon, S. M.; Kim, H. S.; Jin, H. J. *Polymer* **2009**, *50*, 2785.